

Low-loss three-dimensional printed ridge waveguides using stereolithography

Helio Ramollari and Philip Measor^{✉*}

Whitworth University, Microdevices Lab, Engineering and Physics Department,
Spokane, Washington, United States

Abstract. Ridge waveguides were three-dimensional printed using a stereolithography printer and hydrogel resin formulation. The ridge waveguides were 13, 20, and 30 μm wide, 3 to 6 μm high, and 4.4 mm long. The loss of the waveguides was measured using the cutback method and ranged between 0.28 and 1.2 cm^{-1} (or 1.2 and 5.2 dB/cm) with transmittances up to 0.94 (0.27 dB coupling loss) using 635 nm light. Our work demonstrates a quick and inexpensive method to fabricate integrated photonic chips with the promise to fabricate more complex photonic devices and systems. © The Authors. Published by SPIE under a Creative Commons Attribution 4.0 International License. Distribution or reproduction of this work in whole or in part requires full attribution of the original publication, including its DOI. [DOI: [10.1117/1.JOM.2.4.043501](https://doi.org/10.1117/1.JOM.2.4.043501)]

Keywords: three-dimensional printing; integrated waveguide; ridge; chip; stereolithography.

Paper 22017G received Jul. 11, 2022; accepted for publication Nov. 12, 2022; published online Nov. 24, 2022.

1 Introduction

Photonic integrated circuit (IC) devices are utilized in the telecommunications and medical industries.¹ Integrated waveguides, the wire equivalent in electrical ICs, are the most fundamental and critical system component in photonic ICs. Therefore, any improvement in fabrication has wide ranging benefits. One common integrated waveguide is a ridge waveguide, which consists of a ridge patterned on top of a substrate of a lower index.¹ Integrated ridge waveguides are typically fabricated using silicon microfabrication methods with high costs for specialized instruments, masks, cleanroom maintenance, and trained personnel, thereby raising the barrier to entry.² Consequently, alternative polymer waveguides such as polydimethylsiloxane have garnered increased interest.³ Polymer waveguides avoid the deposition and etch steps (reducing instrument costs) using the resin as the waveguide material, but they still have expensive processing steps. An alternative method, three-dimensional (3D) printing or additive manufacturing,⁴ has the potential to disrupt the photonics industry by combining the advantages of polymer waveguides without the need for a cleanroom, masks, highly trained personnel, or multiple expensive instruments. This work explores the use of stereolithography (SLA) 3D printing to fabricate ridge waveguides and demonstrates a method that broadens the reach of integrated photonics.

3D printed (3DP) waveguides for millimeter-wave and THz frequencies, using metallic coatings, have been explored.⁵ However, near-infrared (NIR) and visible light demonstrations have been limited due to 3D printer resolution limits. Recently, 3DP ridge waveguides have been demonstrated using a nozzle-based fused deposition modeling 3D printer with losses as low as 11.86 dB/cm (or 2.73 cm^{-1}) using 632 nm light with a 434- μm wide and 181- μm high ridge waveguide.⁶ To overcome the resolution limit, two-photon absorption methods have been explored to create unique photonic crystal fiber structures and losses of 1.5 dB/cm at 632 nm.^{6,7} Indeed, low-loss and highly miniaturized waveguides are of interest to allow for single-mode operation and higher density to enable complex and compact photonic IC devices. In this work, ridge waveguides with sub-100- μm scale features are demonstrated using SLA and a hydrogel resin formulation.

*Address all correspondence to Philip Measor, pmeasor@whitworth.edu

2 Methods

To demonstrate 3DP ridge waveguides, a custom SLA 3D printer was constructed. The 3D printer used an inverted exposure method and a programmable digital light processing (DLP) ultraviolet light source (digital light innovations). The primary limitations of commercially available 3D printers that were addressed by the custom 3D printer are as follows: lateral (xy) resolutions were limited to 50 to 100 μm (due to spot or pixel size), the layer thickness was limited to 25 to 300 μm (due to stepper motor resolution), and the build volumes were limited to larger scales on the $15 \times 15 \times 20 \text{ cm}^3$ dimensions (instead of the chip-scale structures). The introduction of our custom printer allowed for lateral resolutions down to 10 μm , layer thicknesses of less than 1 μm , and build volumes on the $2.54 \times 2.54 \times 0.05 \text{ cm}^3$ dimensions. The optical path (see Fig. 1) consisted of an ultraviolet-A (UVA, 365 nm) source ($\sim 48.2 \mu\text{W}/\mu\text{m}^2$) directed to a programmable digital micromirror device (DMD), a beam shaping lens system, a mirror (M1), an aperture stage through an optical window, and a Teflon fluorinated ethylene propylene release layer; it then finally exposed the resin. The exposed resin was then polymerized (solidified) onto a substrate attached to the build platform with a piezoelectric-driven z -stage (Thorlabs PIA25, 20 nm resolution).

A hydrogel resin consisting of poly(ethylene glycol) diacrylate and Irgacure 819 photoinitiator was specifically selected for the printer with high absorbance at the UVA exposure range ($\sim 365 \text{ nm}$) for polymerization but maintained optical transparency in the visible and NIR wavelength range.⁸ A UV absorber, avobenzene (Making Cosmetics, Inc.), was selected to control the penetration depth of the resin and other factors discussed elsewhere.⁸ The resin refractive index, across the visible spectrum, was previously characterized to be 1.507 at 635 nm.⁹ To maintain optical confinement laterally, the selected substrate was a thermal oxide layer ($n = 1.450$ from the vendor) grown on a silicon wafer (UniversityWafer, Inc.) and cleaved into a $14 \times 4.4 \text{ mm}^2$ chip. The chip length was limited by the dimensions of the light source and accuracy of cleaving. All of the waveguides were fabricated using a 1-s light exposure time with the entire layer ($\sim 3.5 \text{ cm}^2$) made simultaneously. Waveguides were characterized using a laser source (Thorlabs, pigtailed laser diode, 635 nm) coupled to single-mode fiber (Newport, F-SV, NA = 0.1, $\sim 4 \mu\text{m}$ mode-field diameter), butt-coupled to the 3DP ridge waveguides, and the output was directed to an optical power meter (Thorlabs, S120VC) via an objective lens (Newport, M-20X).

The waveguide loss coefficient α and coupling coefficient κ were measured using the standard cutback method.¹ The transmittance T was measured by determining the input power P_{in} of the butt-coupled fiber and output power P_{out} of the 3DP waveguide determined by the following model:¹

$$T = \frac{P_{\text{out}}}{P_{\text{in}}} = \kappa e^{-\alpha L}, \quad (1)$$

where L is the length of the waveguide. The transmittance was measured for various lengths and the data were fit to

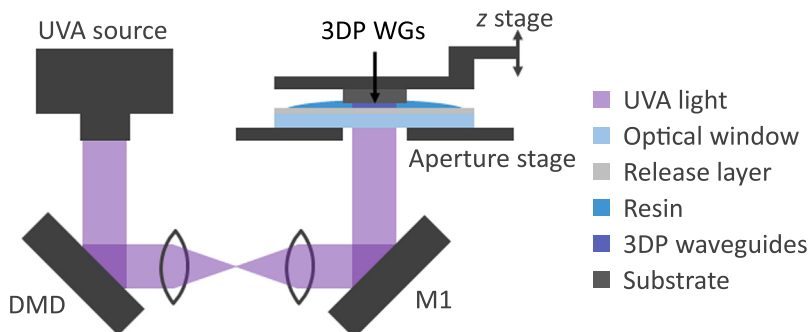


Fig. 1 Custom stereolithographic 3D printer setup.

$$\ln(T) = \ln(\kappa) - \alpha L, \tag{2}$$

where the natural log of Eq. (1) was taken for a more convenient linear fitting expression.

3 Results

To demonstrate 3DP waveguides and characterize performance, sets of lines and spaces were patterned of varying widths corresponding to the current 3D printer pixel size limit (one, two, or three pixels), and the resulting structure resembled standard ridge waveguides (see Figs. 2 and 3). The top-down view (see Fig. 2) shows that most waveguides were intact in this particular structure, but some devices broke off at the end facets and were subsequently excluded from the analysis. The structures also show defects and scratches from the release layer that was transferred into the ridge structure, which could potentially add to the scattering dominated loss.

The waveguide end facets were then imaged and the cross-sectional view showed intact ridge structures with varying amounts of residual resin around the ridges (see Fig. 3).

The waveguides were 13 ± 1.5 , 20 ± 2.3 , and $30 \pm 2.7 \mu\text{m}$ wide and 3.6 ± 0.1 , 4.8 ± 0.1 , and $6 \pm 0.2 \mu\text{m}$ tall, respectively (where the average \pm standard deviation is specified). The

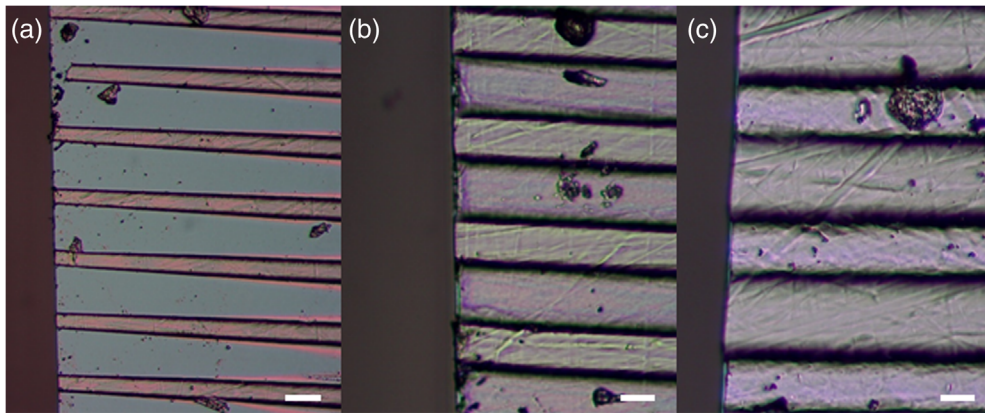


Fig. 2 Top-down view of 3D printed ridge waveguides (a) $13 \mu\text{m}$, (b) $20 \mu\text{m}$, and (c) $30 \mu\text{m}$ wide (scale bars $20 \mu\text{m}$).

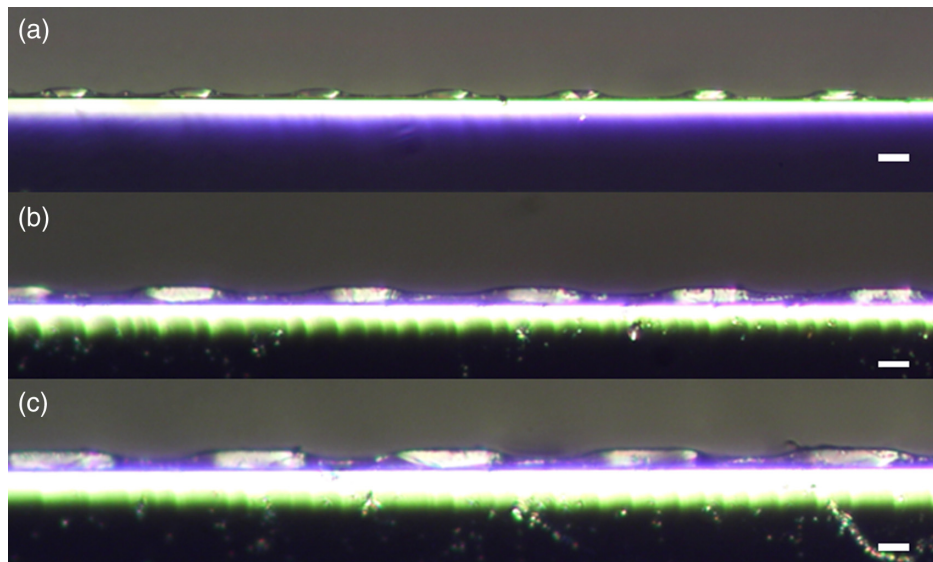


Fig. 3 Cross-sectional side-view of 3D printed ridge waveguides (a) $13 \mu\text{m}$, (b) $20 \mu\text{m}$, and (c) $30 \mu\text{m}$ wide (scale bars $10 \mu\text{m}$).

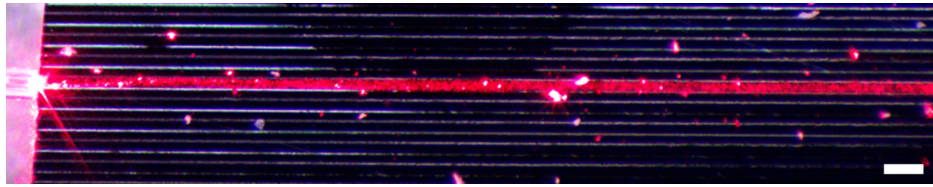


Fig. 4 A 3D printed ridge waveguide (30 μm wide) as viewed from above (100 μm scale bar).

waveguide dimensions were ultimately limited by the fabrication method due to the pixel size of the DMD and could be improved with additional innovation of the commercial light source. The height of the waveguide was limited by the alignment of the substrate to the optical window. As the waveguide width increased, the residual resin on the sides of the waveguide increased. This may be from scattered UVA light as it propagated through the release layer. This possibly could be mitigated by spacing the waveguides further apart or improving the Teflon transparency. Next, 635 nm light was coupled into the waveguides and viewed from above (see Fig. 4).

The light can be seen to be strongly confined within the ridge structure for the entire 4.4 mm length and is not seen coupled to adjacent waveguides. If the loss was large, the intensity of light observed from above would have died out within the first few hundred microns of propagation, but Fig. 4 shows a near constant intensity across several millimeters, demonstrating a low-loss waveguide. Light that is scattered from residual hardened resin on top of the structure and scratches seemed to not significantly affect the waveguide loss; however, this suggests that lower loss could be achieved through further postprocessing steps (see Fig. 4). The side-view of the ridge waveguides [Fig. 5(a)] showed optical confinement within the ridges when light was coupled into the waveguide [Fig. 5(b)].

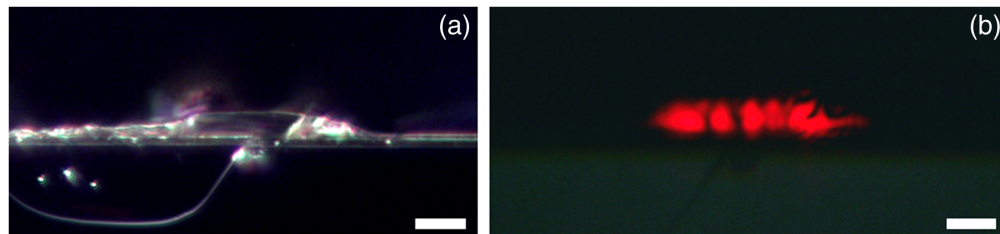


Fig. 5 A 3DP ridge waveguide ($\sim 30 \mu\text{m}$ wide and $6 \mu\text{m}$ high) cross-sectional side-view of (a) output facet (darkfield image, $\sim 10 \mu\text{m}$ scale bar) and (b) corresponding waveguide mode output ($\sim 10 \mu\text{m}$ scale bar).

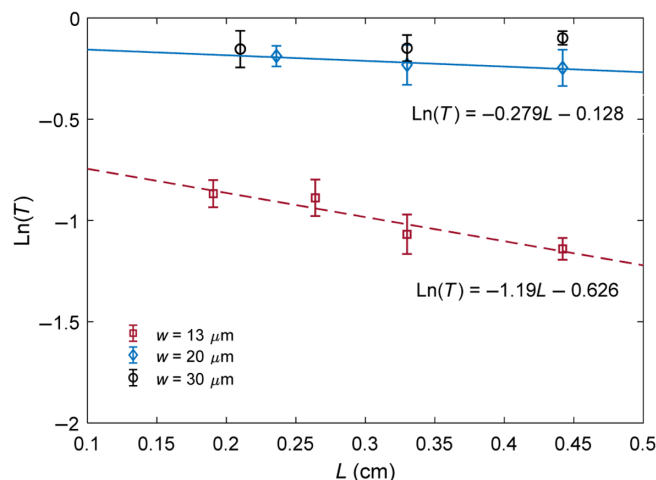


Fig. 6 3DP ridge waveguide cutback loss measurements for various waveguide widths of 13 μm (\square), 20 μm (\diamond), and 30 μm (\circ).

The output exhibited expected multimode behavior, with a fifth-order mode horizontally but single-mode vertically [Fig. 5(b)]. The waveguide loss was determined using the cutback method for 95 waveguides that were $w = 13, 20, \text{ or } 30 \mu\text{m}$ wide and initially a length $L = 4.4 \text{ mm}$ long (see Fig. 6).

The loss coefficients of the 13- and 20- μm wide devices were 1.2 and 0.28 cm^{-1} (or 5.2 and 1.2 dB/cm), respectively, indicating a strong width-dependent loss (as expected for lower confinement and higher scattering losses). The coupling coefficients for the 13- and 20- μm wide devices were 0.53 and 0.88 (or -2.76 and -0.56 dB), respectively; hence the coupling losses were <3 dB. The 30- μm wide waveguide transmittances showed a negative slope, indicating a coupling coefficient dominant loss mechanism rather than a loss coefficient mechanism. Therefore, the loss was too low to measure for this particular waveguide length. Longer waveguides would have been required to characterize the loss of the 30- μm waveguides. However, the transmittances of the 30- μm wide waveguides were consistently high with $T = 0.91 \pm 0.034$ (average \pm standard deviation, 0.94 maximum).

4 Conclusions

Low-loss 3DP ridge waveguides were demonstrated with sub-100- μm dimensions using SLA DLP 3D printing. The losses for the 13- and 20- μm ridge waveguides were 1.2 and 0.28 cm^{-1} , respectively, which are comparable to integrated photonic waveguides made using silicon micro-fabrication methods. Transmittances of up to 94% were achieved using 30 μm wide by 6 μm high waveguides, but the loss was too low to measure for these particular lengths.

This demonstration also broadens the reach of integrated photonics by lowering the training requirements for fabrication and suggests that more complex systems may be possible without a cleanroom. The ability to make ridge waveguide devices within 1 s, without a cleanroom, maskless, with little to no training, and with a single instrument is an attractive prospect. Future research may entail manufacturing waveguides with lower loss, waveguides with single-mode operation, or different kinds of integrated waveguides.

Acknowledgements

We would like to thank Taylor Burchard for help preparing the resins used in this study. The authors would also like to acknowledge the financial support of Whitworth University. This work was previously reported at SPIE Photonics West 2022.¹⁰ The authors declare no conflicts of interest.

References

1. B. E. A. Saleh and M. C. Teich, *Fundamentals of Photonics*, pp. 260–261, Wiley, New York (2000).
2. N. M. Fahrenkopf et al., “The AIM photonics MPW: a highly accessible cutting edge technology for rapid prototyping of photonic integrated circuits,” *IEEE J. Sel. Top. Quantum Electron.* **25**(5), 8201406 (2019).
3. D. A. Chang-Yen, R. K. Eich, and B. K. Gale, “A monolithic PDMS waveguide system fabricated using soft-lithography techniques,” *IEEE J. Lightwave Technol.* **23**(6), 2088–2093 (2005).
4. A. Gebhardt and J. S. Hötter, *Additive Manufacturing*, Hanser Publishers, Cincinnati (2016).
5. B. Zhang et al., “Review of 3D printed millimeter-wave and terahertz passive devices,” *Int. J. Antennas Propag.* **2017**, 1297931 (2017).
6. K. Cook and J. Canning, “3D printing and photonics,” in *Asia-Pac. Opt. Sens. Conf.*, Matsue City, Shimane (2018).
7. T. Blachowicz, G. Ehrmann, and A. Ehrmann, “Optical elements from 3D printed polymers,” *e-Polymers* **21**(1), 549–565 (2021).

8. S. Shrestha, C. Roberts, and P. Measor, "A transparent UVA-1 biocompatible photoresin towards 3D printed lab-on-a-chip," in *Murdock Coll. Sci. Res. Conf.*, Vancouver, Washington (2019).
9. M. Reynoso, I. Gauli, and P. Measor, "Refractive index and dispersion of transparent 3D printing photoresins," *Opt. Mater. Express* **11**(10), 3392–3397 (2021).
10. H. Ramollari and P. Measor, "A low-loss 3D printed ridge waveguide via stereolithography," *Proc. SPIE* **12004**, 120040S (2022).

Helio Ramollari is an undergraduate general engineering student at Whitworth University. He joined the Microdevices Lab at Whitworth University in 2021. His research interests are in 3D printed integrated waveguides and biosensors. He anticipates graduating in 2023 and plans to pursue his PhD studies in integrated photonics and its applications. He is a student member of SPIE.

Philip Measor received his PhD in electrical engineering from the University of California Santa Cruz in 2010. He is an assistant professor in the Engineering and Physics Department at Whitworth University and founded the Microdevices Lab. Prior to academic appointment, he was a research scientist at KLA Tencor Corp., a leader in semiconductor process control. Before the semiconductor industry, he founded a biotechnology start-up company, LiquiLume Diagnostics, Inc., that explored the commercialization of optofluidic devices and innovative waveguides. He is the author of more than 45 journal papers and conference proceedings and has 8 patents in the fields of integrated optics, optofluidics, biosensing, and semiconductor process control. His current research interests include additive manufacturing of microdevices, including integrated waveguides and microfluidic devices, for various applications, such as biosensing, infectious disease detection, and micro-organism analysis. He is a member of SPIE.